



# Hourly day-ahead wind power forecasting at two wind farms in northeast Brazil using WRF model



William Duarte Jacondino <sup>a,\*</sup>, Ana Lucia da Silva Nascimento <sup>b</sup>, Leonardo Calvetti <sup>a</sup>, Gilberto Fisch <sup>b</sup>, Cesar Augustus Assis Beneti <sup>c</sup>, Sheila Radman da Paz <sup>c</sup>

<sup>a</sup> Federal University of Pelotas (UFPel), Av. Idefonso Simões Lopes, 2751, 96060-290, Pelotas, Brazil

<sup>b</sup> National Institute for Space Research (INPE), Av. Dos Astronautas, 1758, São José Dos Campos, Brazil

<sup>c</sup> Sistema Meteorológico Do Paraná (SIMEPAR), Av. Francisco H. Dos Santos, 210, 81531-980, Curitiba, Brazil

## ARTICLE INFO

### Article history:

Received 10 March 2021

Received in revised form

25 April 2021

Accepted 2 May 2021

Available online 6 May 2021

### Keywords:

WRF

Onshore

Forecast

Wind power

Brazil

## ABSTRACT

Wind energy is rapidly growing industry in Brazil. Wind speed forecasting is necessary in the planning, controlling, and monitoring for the reliable and efficient operation of the wind power systems. Thus, this study focuses on the impact of different physics parameterization in forecasting wind speed in two onshore wind farms using the Weather and Research Forecasting (WRF) model. The wind farms are located in Parazinho, in the northeast of Brazil, a region with high wind resource. Hindcasts are performed for a high (i.e., July 2017) and low (i.e., April 2017) wind speed regimes using different forecast lead-times (i.e., 24–48 h). The best performing setup consists of Thompson microphysics, Bougeault-Lacarrere PBL, Betts-Miller cumulus, New Goddard Longwave/Shortwave radiation, and Pleim-Xiu Land Surface schemes. Our findings also suggest that the model forecast setting with the TKE closure scheme, namely BouLac, performed better than that setting with first-order closure ACM2. The best mean monthly error (MAE) obtained is  $1.1 \text{ m s}^{-1}$  for wind and 12.6% for wind power.

© 2021 Elsevier Ltd. All rights reserved.

## 1. Introduction

Renewable energy sources such as wind and solar is increasingly present in the global electric matrix, driven mainly by technological advances and its cost-competitive in the last two decades [1]. Among these, wind power that is given by the harnessing of kinetic energy contained in moving air masses (wind) is one of the most has been highlighted in alternative energy sources. Currently in Brazil, wind power installed capacity stands at 18 GW and already represents 9.7% of the Brazilian electric matrix [2]. About 85% of wind power generation that is injected into the National Interconnected System (SIN) comes from the Northeast Region of the country, favored by the regularity of constant winds of moderate to strong intensity and practically unidirectional throughout the year (Trade Winds) [2].

The rapid growth of wind energy in the Brazilian electric system worries the operating sector due to uncertainties in the power generation inherent to wind power plants, which are directly

dependent on wind speed variability (spatial and temporal) [3]. Electrical system operators need to continuously maintain the balance between power demand and the total power generated by the power plants responsible for supplying the system. Large errors in wind speed estimates can compromise the dispatch planning and operation of electrical system. However, predicting wind energy production can be a quite challenging task due to complex fluctuations in the speed of wind [3]. In an attempt to mitigate some of these problems, accurate forecasts covering several time scales become fundamental to assist the operational management of wind farms and the electrical system. Short-term forecasts (30 min–72 h) are often of greater interest to decision makers in the operating sector, mainly because it helps in the economic dispatch of energy and the commercialization of energy in the day-ahead market [3,4].

There is a vast amount of literature on approaches and techniques for wind speed forecast and its associated wind power generation, being the use of numerical models such as the Weather Research and Forecasting Model (WRF) one of the most used to this end. WRF is a meso-scale model that allows the use of different numerical and physical options together to describe the behavior of atmospheric evolution of various meteorological phenomena and

\* Corresponding author.

E-mail addresses: [wiliamjacondinoufpel@gmail.com](mailto:wiliamjacondinoufpel@gmail.com), [wiliamjacondino@hotmail.com](mailto:wiliamjacondino@hotmail.com) (W. Duarte Jacondino).

physical processes that occur at different time-space scales. Most of the studies point out that wind forecast is highly sensitive to the use of different physical schemes (parameterizations) of planetary boundary layer (PBL) and land surface models (LSM) [5–12]. In fact [10], showed that the wind forecast at 30 m above ground level (m AGL) in the state of Alagoas (Northeast Region of Brazil) presents a bias strongly dependent on the seasonality of the region, and the uncertainties in the forecast increases during the transition period from dry to rainy season. The literature shows that forecasting the near surface wind is still a challenge and presents a dependence on the type of topography (homogeneous or heterogeneous) [13,14]. The errors and uncertainties of the model are also correlated with the increased complexity of the terrain [15,16]. However, the number of studies that evaluates wind forecast at turbine height (>80 m AGL) for the Northeastern Region of Brazil are still limited, height that corresponds to turbulent flows of momentum, heat and moisture highly variable and dependent on time of day, season and atmospheric stability.

In this context, this paper seeks to evaluate the performance of WRF model (version 3.9.1.1) for wind speed forecasting at 95 m AGL and its associated wind energy in two wind farms located in Parazinho (Northeast Region of Brazil). Model accuracy is evaluated for two forecast lead times (24 and 48 h) during two distinct periods: one representative of strong winds (dry period) and another of weak winds (rainy period), respectively September and April 2017 [17]. In addition, a sensitivity analysis with several experiments was conducted to verify the performance of the model against different physical options. The sensitivity of numerical experiments aims to compare and preliminarily evaluate which physical options best fit the wind forecast in the study region. This manuscript is structured as follows: in addition to this introduction, Section 2 describes the study area and the data set used; Section 3 describes the set-up adopted for WRF model, the sensitivity experiments and the measures used to evaluate the forecasts; Section 4 presents a detailed analysis and discussion of the errors for both forecasting horizons, and finally, Section 5 presents the main conclusions of this study.

## 2. Data and methodology

### 2.1. Study area

The study area comprises two wind farms located in the municipality of Parazinho, in the state of Rio Grande do Norte (Northeast Region of Brazil) between latitudes 5°23'52.3"S and 5°16'36.6"S and longitudes 36°04'35.4"W and 35°50'00.1"W. Wind farms may not have their names revealed because of data confidentiality reasons, so the anemometric masts will be referenced as A1 and A2. The climate in Parazinho is tropical semi-arid [18]. In the global context, this region is inserted in the intertropical zone of the globe, closer to the equator than the tropics. The region is also subject to the action of the seasonal movements of the Intertropical Convergence Zone (ITCZ), with the seasons being defined according to the rainy and dry periods and not by the seasonal differences in temperature, since there has low thermal amplitudes [19]. In addition, the city of Parazinho is located approximately 56 km off the east coast of Northeast Brazil, being subject to the influence of sea breezes when coupled with other systems. The atmospheric dynamics in the region is strongly influenced by the Trade Winds [20], which makes this region one of the most productive for wind energy. In Brazil, the state of Rio Grande do Norte is currently the leader in onshore wind energy, with more than 181 wind farms distributed over the region which together sums up for 5.1 GW of the total installed capacity in operation in the country [2].

### 2.2. In-situ wind measurements

The measured wind speed and direction data were collected by a high precision Thies First Class cup anemometer (1% of the measured value or 0.2 m s<sup>-1</sup>, whichever is greater), and a Thies Compact wind vane [21], respectively, installed on each mast at 95 m AGL. Wind speed and direction data correspond to the hourly-average (local time - HL) of the measurements that are taken at a frequency of 1 Hz and integrated at 10-min intervals, comprising the period from April 1 to April 30, 2017 (representative month of the region's rainy season) and from September 1 to September 30, 2017 (representative month of the region's dry season). A quality control was performed on the raw observed data before using it for validation, filtering out discontinuities and missing data. After the data evaluation process, data availability equivalent to 99.9% was obtained. More details about data quality control can be found in Ref. [17].

## 3. WRF configuration and model validation

### 3.1. Model configuration and sensitivity experiments

This study used the WRF-ARW model version 3.9.1.1 in non-hydrostatic mode to produce short-term wind speed forecasting. WRF is a mesoscale numerical model widely used in the scientific community for atmospheric research. More details about the model can be found in Ref. [22]. A two-way nesting domain configuration was adopted to ensure information exchange between the three domains used (see Fig. 1). The outer domain (D1) has a grid spacing of 9 km and 141 × 141 grid points in each horizontal direction. The first nested grid has 3 km (D2) spacing with 127 × 127 grid points in horizontal direction. The inner grid has 1 km (D3) of spacing with 115 × 115 grid points in each horizontal direction with a time step of 3 s and outputs every 10 min. The vertical grid is the same for all domains, with 67 vertical layers, being the first 8 and 34 levels respectively comprised in the first 100 and 2000 m AGL. The initial and boundary conditions is taken from the forecast data provided by the Global Forecast System (GFS), with a spatial resolution of 0.25° × 0.25° and 3 h update interval, which are publicly available at <https://rda.ucar.edu/datasets/ds084.1/#!description>. The reason for using forecasting data and not analysis is to fulfill the goal of determining the predictability of the model, placing it in an operational scenario. The physical composition of the Earth's surface was configured through USGS (United States Geological Survey - <http://www.usgs.gov>) topography and MODIS (Moderate Resolution Imaging Spectroradiometer - <https://modis.gsfc.nasa.gov/>) vegetation, both with 30 arc second elevation dataset (925 m).

For this study, two forecasting steps with the WRF were performed. The first step consists on the evaluation of 32 sensitivity experiments (for each month) to find the most suitable set of parameterization schemes that presents the best performance for wind prediction in our study region. A series of experiments were performed in this study, starting from a control (default) run (Fig. 2A), changing one option at a time listed for each physic parameterization in Fig. 2B. The period chosen for the sensitivity experiments goes from April 2nd to 5th (rainy period) and September (dry period) of 2017 to meet the goal of evaluating the model performance during two contrasting seasonal regimes of wind speed. For both periods and each sensitivity experiment the model is run for 63 h (15 h spin up + 48 h forecast), starting at 12 UTC on the previous day from GFS forecast data. The cumulus scheme was turned off in domains 2 (3 km) and 3 (1 km), being activated only in domain 1 (9 km), since for grid spacing smaller than 5 km the model should be able to explicitly resolves deep convection processes [23–25]. Only the results of the highest

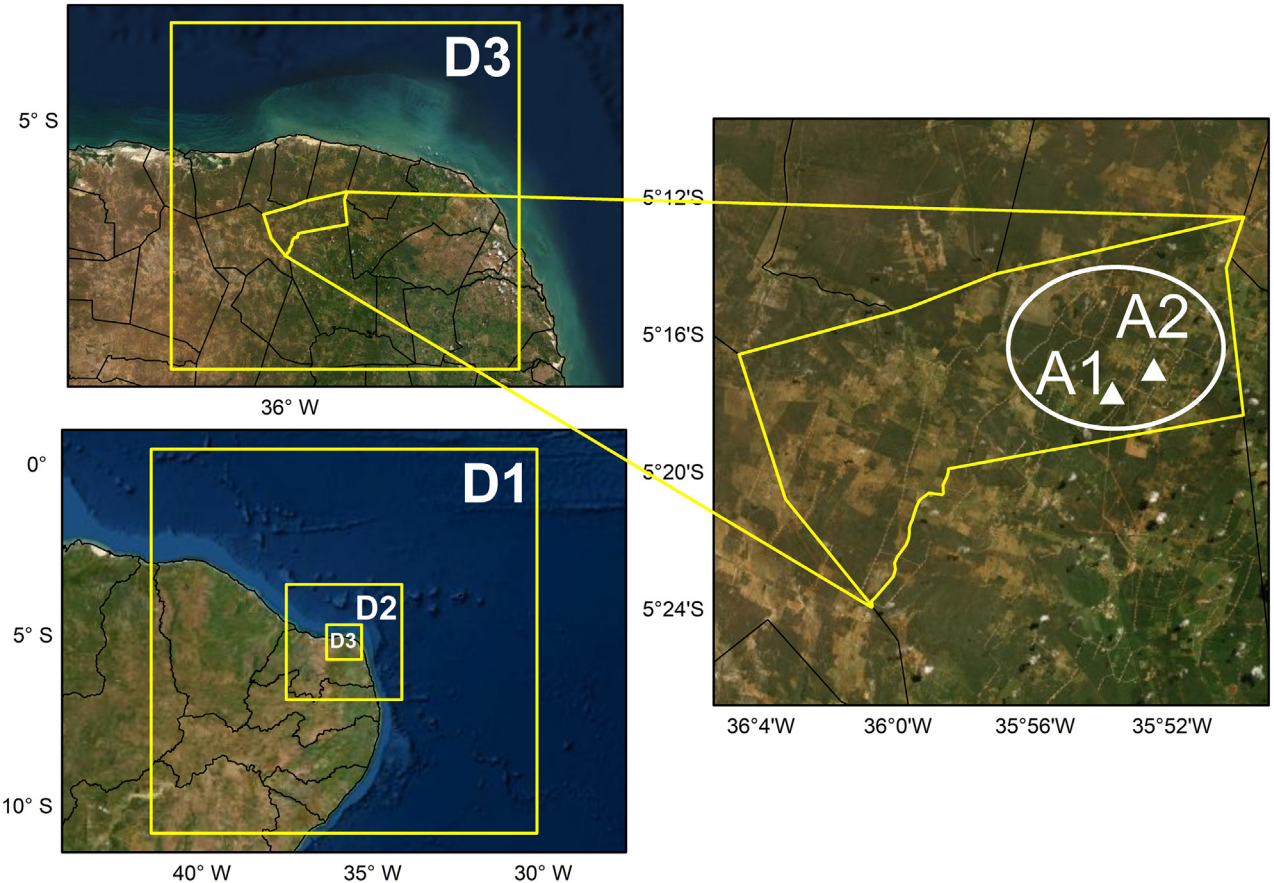


**Fig. 1.** Model domains with the horizontal grid size of 9 km (D1), 3 km (D2), and 1 km (D3) centered over Parazinho (yellow solid line in D3). Wind farm locations is presented for the D3 inset map (white triangle). (For interpretation of the references to colour in this figure legend, the reader is referred to the Web version of this article.)

resolution domain (1 km) were extracted to evaluate forecasts performance. The second step consists of forecasting wind speed and wind energy covering the whole month of April (2017-04-01 - 2017-04-30) and September (2017-09-01 - 2017-09-30), broken into 30 daily forecasts (for each month). Thus, forecasts were made from two configurations composed by the combination of the best physical parameterization schemes defined during the sensitivity tests. The model performance is then evaluated for both forecast lead times (24 and 48 h). During the post processing, as our observed data are in local time and the model outputs are in UTC time, to correctly compare them the following relationship was adopted: Local time (HL) = UTC time - 3 h.

### 3.2. Post-processing of wind data from WRF output files

A position (specified as latitude (*i*), longitude (*j*), and vertical level (*k*) on the WRF grid corresponds to a cell. Wind speeds and directions for a position in WRF were calculated from the U (x-component) and V (y-component) winds. The U winds are on at the centres of the left and right faces of the cell, while the V winds are on the middles of the front and back faces as illustrated in Ref. [26]. The forecasted winds that were used for analysis was calculated (on an hourly basis) using a vector approach as:

$$\text{Speed} = \left[ \left( \frac{U_{i,j,k} + U_{i+1,j,k}}{2} \right)^2 + \left( \frac{V_{i,j,k} + V_{i,j+1,k}}{2} \right)^2 \right]^{0.5} \quad (1)$$

Direction was determined from the same hourly U and V

averages using the four-quadrant inverse tangent formular.

The wind speeds at the tower height of analysis (95 m) were interpolated from the wind speeds for the levels immediately below and above them. For this, the vertical levels in WRF had to be converted to height above ground level (in m). These were calculated hourly according to Refs. [26,27] as:

$$\text{Height} = \left( \frac{(PH + PHB)_{i,j,k} + (PH + PHB)_{i,j,k+1}}{2g} \right) - HGT \quad (2)$$

where PH is the perturbation geopotential height, PHB the base-state geopotential height, and HGT, the terrain height [26,27]. Values for PH, PHB and HGT were all obtained from the forecast results.

### 3.3. Model validation

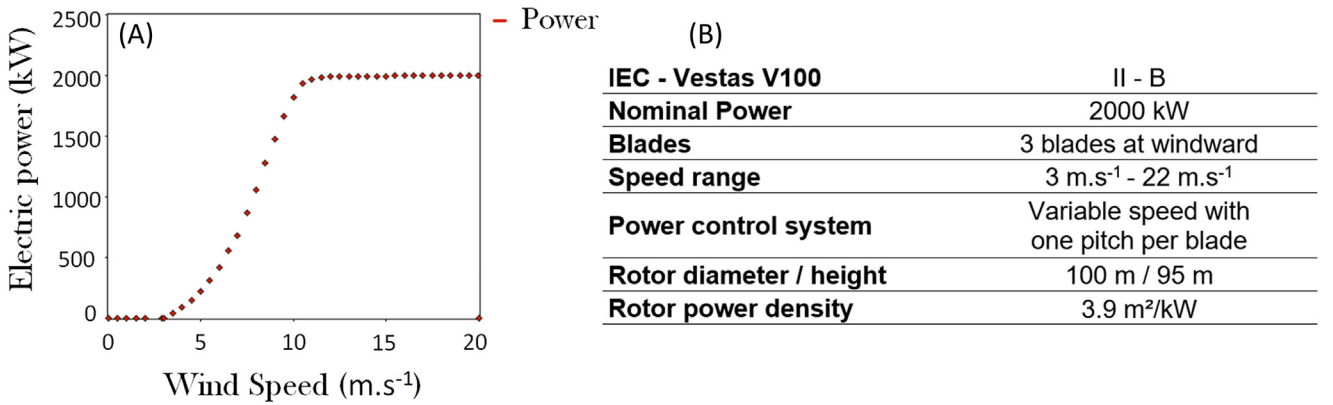
In order to assess the WRF model forecasting skills with respect to the wind speed the following indexes were calculated: BIAS (Equation (3)), Root Mean Square Error (RMSE) (Equation (4)), Mean Absolute Error (MAE) (Equation (5)), Mean Absolute Percentage Error (MAPE) (Equation (6)) and the Pearson correlation coefficient (*r*) (Equation (7)). With respect to wind energy production, the Vestas V100–2.0 MW wind turbine model was considered [28]. This is the same type of wind turbine that is used in the wind farms (A1 and A2). The main characteristics of this wind turbine and its power curve is presented in Fig. 3. The errors associated to wind energy were calculated as a function of the turbine capacity (in a percentage scale), by the Normalized Mean

(A)	Physical Process	Parameterization scheme		
	<i>Microphysics</i>	WSM3		
	<i>Longwave Radiation</i>	RRTM		
	<i>Shortwave Radiation</i>	Dudhia		
	<i>Surface Layer</i>	Revised MM5 Monin-Obukhov		
	<i>Land Surface</i>	Noah LSM		
	<i>Planetary Boundary layer</i>	Yonsei University		
	<i>Cumulus Parameterization</i>	Kain-Fritsch		

(B)	Parameterization scheme	Physical options		
<i>Microphysics</i>	WSM3	Kessler	Lin	
	WSM5	Ferrier	WSM6	
	Thompson	Morrison	WDM6	
<i>Longwave Radiation</i>	RRTM	RRTMG	New Goddard	
<i>Shortwave Radiation</i>	Dudhia	RRTMG	New Goddard	
<i>Cumulus</i>	Kain-Fritsch	Betts-Miller	Grell-3D	
	Grell-Devenyi	Cumulus-off		
<i>Planetary Boundary layer</i>	YSU	MYJ	QNSE	
	MYNN 2.5	MYN 3rd	ACM2	
	BouLac	UW	Shin-Hong	
	GBM	MRF		
<i>Land Surface</i>	Noah LSM	Thermal diffusion	RUC LSM	
	Pleim-Xiu			

**Fig. 2.** Physical characteristics of the control run (A) and (B) parameterizations used in the sensitivity analysis.



**Fig. 3.** (A) Vestas V100 - 2 MW wind power curve (The red line represents power). (B) Summary table with the main wind turbine characteristics. Obtained from Ref. [26]. (For interpretation of the references to colour in this figure legend, the reader is referred to the Web version of this article.)

Absolute Error (NMAE) (Equation (8)) and the Normalized Root Mean Square Error (NRMSE) (Equation (9)).

$$BIAS = \frac{1}{N} \sum_{i=1}^N (V_i^{pre} - V_i^{obs}) \quad (3) \quad MAE = \frac{1}{N} \sum_{i=1}^N |V_i^{pre} - V_i^{obs}| \quad (5)$$

$$RMSE = \sqrt{\frac{1}{N} \sum_{i=1}^N (V_i^{pre} - V_i^{obs})^2} \quad (4) \quad MAPE = \frac{1}{N} \sum_{i=1}^N \left| \frac{V_i^{pre} - V_i^{obs}}{V_i^{obs}} \right| \times 100 \quad (6)$$

$$r = \frac{\sum_{i=1}^N (V_i^{pre} - \bar{V}_i^{pre}) (V_i^{obs} - \bar{V}_i^{obs})}{\sqrt{\sum_{i=1}^N (V_i^{pre} - \bar{V}_i^{pre})^2 \sum_{i=1}^N (V_i^{obs} - \bar{V}_i^{obs})^2}} \quad (7)$$

$$NMAE = \frac{1}{N} \sum_{i=1}^N |V_i^{pre} - V_i^{obs}| \times \frac{100}{C_{turbine}} \quad (8)$$

$$NRMSE = \sqrt{\frac{1}{N} \sum_{i=1}^N (V_i^{pre} - V_i^{obs})^2} \times \frac{100}{C_{turbine}} \quad (9)$$

In these equations,  $i$  represents point in time,  $n$  is the total number of such points,  $C_{turbine}$  is the wind turbine capacity, and  $V_i^{pre}$  and  $V_i^{obs}$  are the predicted and observed values, respectively.

## 4. Results and discussion

### 4.1. Evaluation results of sensitivity analysis

First, we tested the performance of the WRF model under the use of different physical options for the highest resolution grid (D3). Figs. 4 and 5 presents the main results obtained in the sensitivity analysis. Thus, different options of PBL parameterization schemes were assessed firstly keeping all other model options at their default values. As shown in Fig. 4, most of the PBL schemes tested have the tendency to overestimate the wind speed. The magnitude of systematic errors for wind forecast is higher in the dry season (September) in A2, especially in the MYJ, MYNN 2.5 and MRF schemes that showed the highest overestimations (BIAS greater than  $2 \text{ m s}^{-1}$ ) (Fig. 4A). Among the eleven PBL schemes tested, the one-and-a-half order, local turbulence kinetic energy (TKE) closure scheme (BouLac) was the one that shows the best performance in terms of wind speed forecasting (low-BIAS values for both periods) (Fig. 4A). The temporal evolution of wind speed is slightly better represented by the MYJ scheme in September ( $r = 0.7$ ), while for April month it is quite unpredictable ( $r \leq 0.5$ ), regardless of PBL scheme chosen (Fig. 4B). The increase of phase errors in April month are possibly connected to the random turbulent vortices that occur more frequently in this period of the year in the study area, which as mentioned by Ref. [29], still need to be better represented in numerical models. Regarding the RMSE, the BouLac experiment showed better performance in wind forecast, with errors less than  $1.7 \text{ m s}^{-1}$  in both months (Fig. 4C). The ACM2 experiment performed second best for all of the statistical metrics (RMS less than  $2.1 \text{ m s}^{-1}$ ). On the other hand, some forecasts

diverged reasonably from observed values, the MRF, MYNN 2.5 (RMSE  $> 3 \text{ m s}^{-1}$ ), MYNN 3rd (RMSE  $> 2.4 \text{ m s}^{-1}$ ) and MYJ (RMSE  $> 2.4 \text{ m s}^{-1}$ ) schemes performed generally worst among the 11 schemes tested in our study (Fig. 4C). According to Ref. [30] errors between 1 and  $2 \text{ m s}^{-1}$  in wind speed can be considered acceptable for applications in wind resources. However, for a realistic forecast of wind power production the ideal is that these errors oscillate around  $1 \text{ m s}^{-1}$ . A 10% error in wind forecast would imply an error of 30% in wind power estimates, so the proper choice of a physical configuration that adjusts to the weather conditions of a given region of interest needs to be investigated.

A similar comparison is shown in Fig. 5, this time for the microphysics sensitivity tests (nine schemes), keeping all other options of the model at their default values (Fig. 2A). Although the differences between the nine microphysics schemes tested are small (from the order of the first to the second decimal place), one out of 9 schemes stand out as more sensitive than others. The results indicate that the Thompson scheme performs slightly better than the other schemes in every measure of wind speed forecast, producing the smallest RMSE and minimum absolute value of mean BIAs (Fig. 5A, C). This scheme explicitly predicts the mixing ratios of five species of liquid and ice (cloud water, snow and graupel), besides being the only single moment scheme that varies the concentration of ice and rain [31].

The third group of experiments involved Land surface parameterization schemes (4 experiments) shown in Fig. 5. A Land-surface model predicts soil temperature and soil moisture in layers (4 for Noah-LSM, 5 for thermal diffusion, 6 for RUC-LSM, and 2 for Pleim-Xiu) and plays an important role in the exchange of heat, moisture and momentum between surface and atmosphere, as well as interacting directly with the other schemes. It is clear from Fig. 5A and C that the wind speed was best represented by the experiment with Pleim-Xiu scheme (lower values of BIAs and RMSE) for both months. The Pleim-Xiu scheme was also the one that presented the best temporal evolution of wind speed for April month ( $0.5 \leq \text{Pearson} \leq 0.7$ ), while during the month of September it was the RUC scheme that performed better (Fig. 5B). A surprising result was that the Noah-LSM scheme presented the greatest errors, exceeding  $2 \text{ m s}^{-1}$  in September (Fig. 5C). Noah-LSM is widely used as default by the research community, and although some authors pointed out that this scheme is the best to represent the surface temperature [32,33], it is not suitable for other parameters (such as wind), at least not for our area and study period according to the results obtained in our sensitivity experiments.

The next group of experiments assessed three combinations of shortwave and longwave radiation schemes. The experiment with the New Goddard option scheme showed the best agreement with the observations in comparison with the others schemes (Fig. 5C). Finally, we analyze the sensitivity of the activation (or not) of the

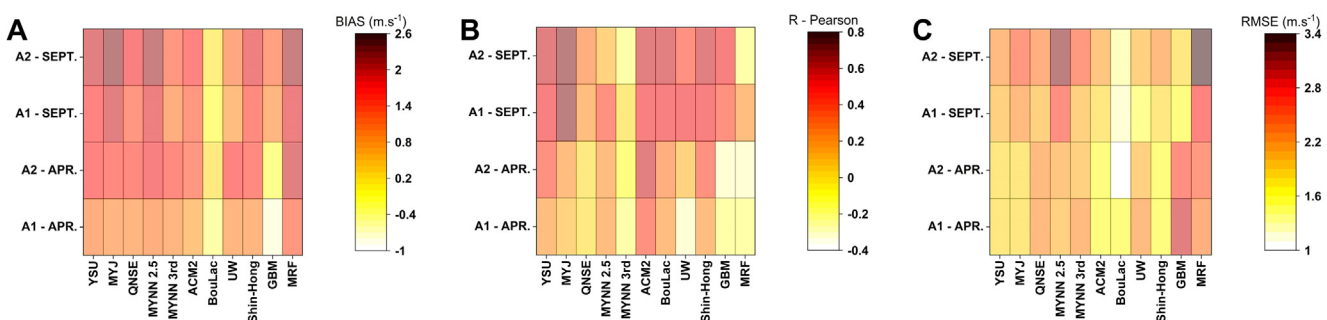
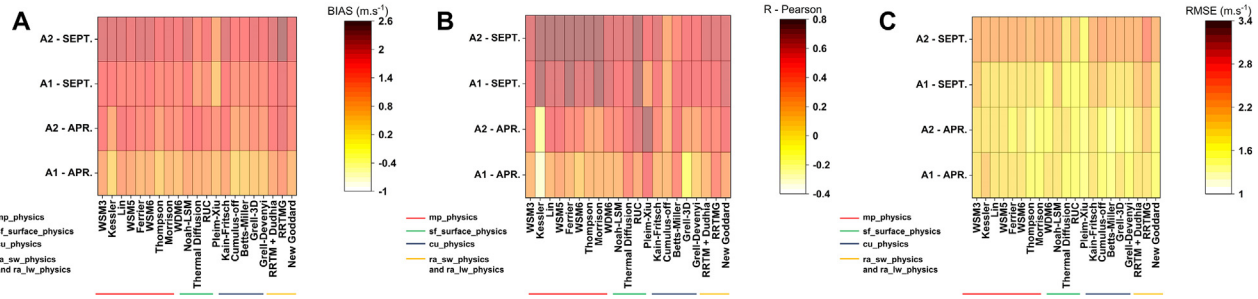


Fig. 4. BIAs, Pearson correlation and root means score for the A1 and A2 experiment areas in april and september 2017 using different planetary boundary layer options.



**Fig. 5.** BIAS, Pearson correlation and root means score for the A1 and A2 experiment areas in april and september 2017 using different physics options.

cumulus parameterizations on the 9 km resolution domain. As can be seen in Fig. 5, the Betts-Miller scheme showed the best behavior regarding BIAS and RMSE for both months (Fig. 5C). An interesting result was that the skill of the experiment in which the cumulus parameterization was turned off performed better than the Kain-Fritsch and Grell-3D schemes turned on in the 9 km resolution domain (during the month of April only). In general, keeping the cumulus parameterization turned on in the 9 km grid seems to perform slightly better than keeping it off.

It is worth mentioning that the schemes that obtained the best performance in our sensitivity analysis are not the commonly options adopted in relevant references for Brazil and other countries. Most of the studies with WRF adopt a pre-established configuration based on previous studies, often without investigating whether the physical options chosen are the most appropriate for the study area. Thus, the present analysis aims to preliminarily identify which schemes were best suited to forecast wind speed in the study area and recommend its use on regions with similar geographic and climate characteristics. The results in our sensitivity analysis show that the wind forecast appears to be more sensitive to the choice of PBL schemes, which may lead to a difference of more than  $2 \text{ m s}^{-1}$  depending on the scheme used. In this way, two distinct physical configurations were considered to forecast the entire months of April and September 2017: one with the BouLAC PBL scheme (hereafter EXPBouLAC), and the other with the ACM2 PBL scheme (hereafter EXPACM2), keeping all other parameterization schemes fixed (see Table 1).

#### 4.2. Evaluation of 95-m wind forecasts

Fig. 6 shows wind speed forecast and corresponding measured (observed) data for both EXPBouLAC and EXPACM2 experiments during the month of April. As can be seen in Fig. 6, the EXPBouLAC is the one that shows the lowest systematic errors (BIAS close to zero) throughout the forecast period for both forecast lead times, while the EXPACM2 showed a strong tendency to overestimate wind speed ( $\text{BIAS} \geq 1.5 \text{ m s}^{-1}$ ). The abrupt decline in wind speed observed between 8 and 11 April is well captured by the model in the EXPBouLAC (Fig. 6A), while the EXPACM2 seems to anticipated the event occurrence, besides overestimating its intensity (Fig. 6B). There are, however, systematic phase errors of wind speed

forecasts in both experiments throughout the April month, which are more frequently in EXPACM2. Such phase errors may be related to the poor representation of some topographical features in the model, which in fact is common in numerical modeling, as pointed by Ref. [9]. Regarding the MAE evaluation, in A1 errors vary between  $1.8 \text{ m s}^{-1}$  on the EXPBouLAC and increases to  $2.1 \text{ m s}^{-1}$  in the EXPACM2 for both forecast lead times. For the A2 wind farm, MAE is reduced by  $0.7 \text{ m s}^{-1}$  (MAE of  $1.1 \text{ m s}^{-1}$ ) in the EXPBouLAC compared with the  $0.3 \text{ m s}^{-1}$  (MAE of  $1.8 \text{ m s}^{-1}$ ) of EXPACM2. EXPBouLAC also showed a considerably lower monthly mean RMSE ( $\sim 1.8 \text{ m s}^{-1}$ ) compared to EXPACM2 ( $\sim 2.2 \text{ m s}^{-1}$ ) in both forecast lead times (April). In fact, MAPE values on EXPBouLAC shows a significant average performance improvement of 10% in comparison to the EXPACM2.

Fig. 7 shows the same as in Fig. 6, but for September 2017. All statistic's metrics show improvements as a result of the season change from autumn (April) to spring (September), when winds become stronger and less variable. The forecasts exhibited strong positive biases in the EXPACM2 (around  $1.4 \text{ m s}^{-1}$ ), while biases close to zero were found in EXPBouLAC, ranging from  $-0.4 \text{ m s}^{-1}$  during the 24 h forecast lead time to  $-0.2 \text{ m s}^{-1}$  during the 48 h forecast lead time. Although the magnitude of the errors for each experiment was comparable, the EXPBouLAC tends to reduces the overestimation of wind speed, especially for maximum wind peaks (Fig. 7). In general, the results indicated that the real-time forecasting with the EXPBouLAC performed better with short forecasting lead times (24 h) than longer ones (48 h), with RMSE around  $1.5 \text{ m s}^{-1}$  and MAPE of 15%. Therefore, the comparison between the experiments suggests that the errors show a dependence on season, and that the proper choice of PBL scheme can improve forecast BIAS and accuracy.

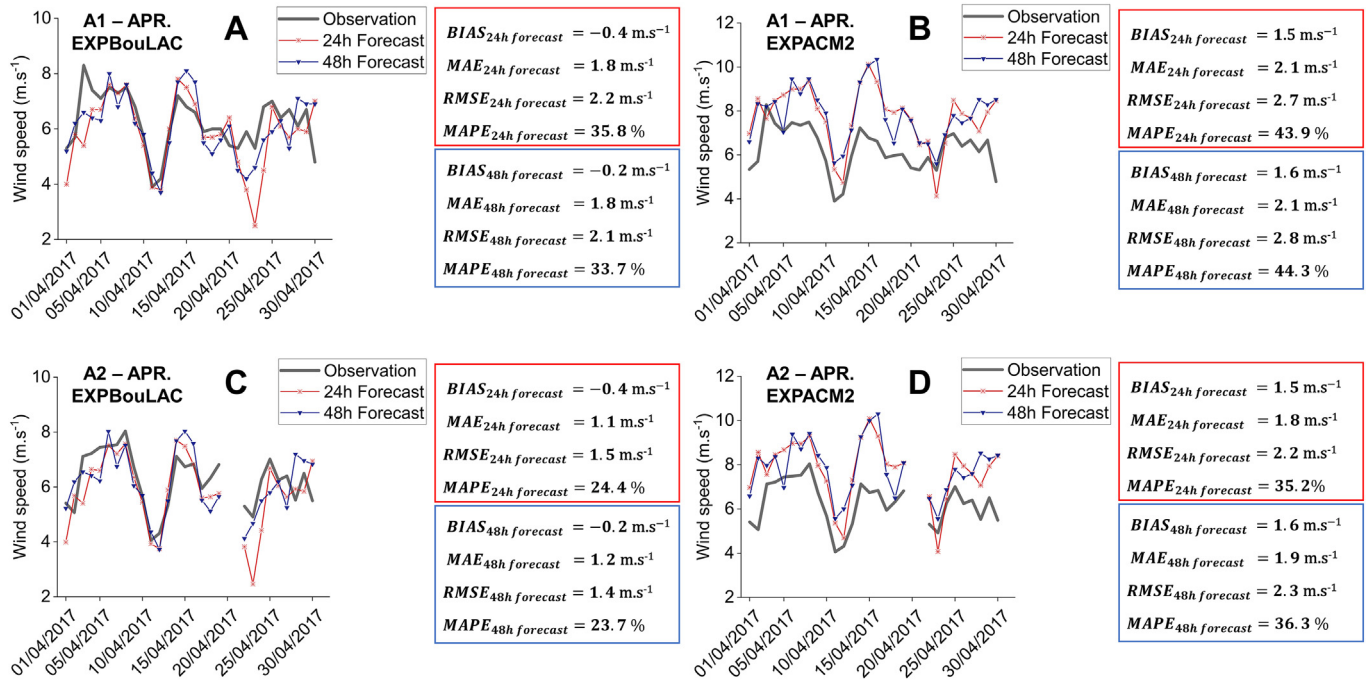
#### 4.3. Evaluation of wind direction predictions

Fig. 8 present monthly-averaged hourly wind roses for each experiment, for April and September months. The wind direction is reasonably well captured by the model on both experiments, although some biases were identified. The prevailing wind directions at both sites is dominated by the southeast sector (Trade Winds) and this is well captured by both experiments as well. The mean wind direction BIAS is found to range between  $\pm 10^\circ$ ,

**Table 1**

Overview of the WRF model experiments used in the present study.

Configuration name	Physics Scheme					
	Planetary Boundary layer	Microphysics	Land Surface	Cumulus	Longwave and Shortwave Radiation	Surface Layer
EXPBouLAC	BouLAC	Thompson	Pleim-Xiu	Betts-Miller	New Goddard	Revised MM5 Monin-Obukhov Pleim
EXPACM2	ACM2	Thompson	Pleim-Xiu	Betts-Miller	New Goddard	



**Fig. 6.** (A,B) Monthly wind speed forecast with BIAS, MAE, RMSE and MAPE statistics for april month at A1 and (C,D) at A2. Results for two WRF configurations (EXPBouLAC and EXPACM2) and different forecast lead times (24 and 48 h) are presented.

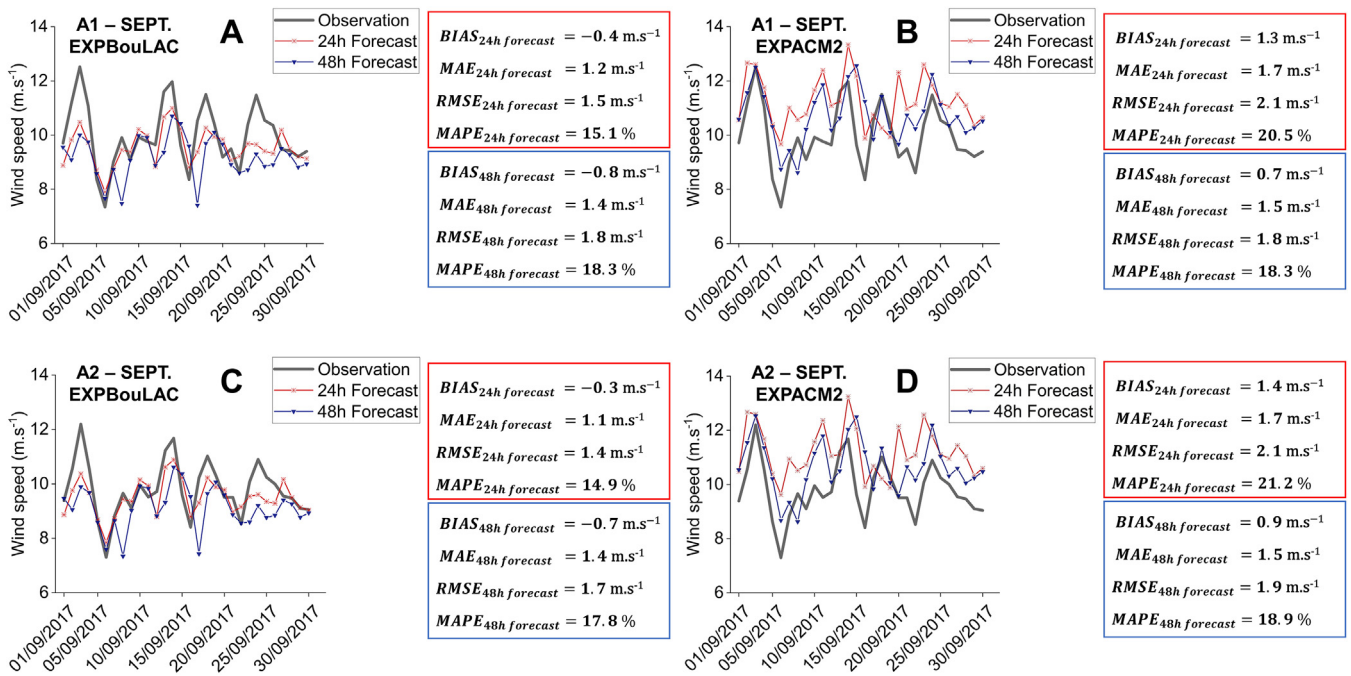


**Fig. 7.** (A,B) Monthly wind speed forecast with BIAS, MAE, RMSE and MAPE statistics for september month at A1 and (C,D) at A2. Results for two WRF configurations (EXPBouLAC and EXPACM2) and different forecast lead times (24 and 48 h) are presented.

depending on season, with mean biases of  $-6^\circ$  (April) and  $+4^\circ$  (September) (Table 2). Thus, there is no high differences in forecast accuracy between EXPBouLAC and EXPACM2 and it is less dependent on lead time. The RMSE is about  $29^\circ$  ( $6.8^\circ$ ) in April (September), yielding a relative MAPE of 21.5% (4.9%). This difference could be related to the higher variability that the wind direction shows for low-wind regimes in April, which makes its

forecast more complex and difficult. On the contrary, high-wind situations (September) show a more defined circulation pattern, and the reproducibility of the wind direction increases, as pointed by Ref. [34].

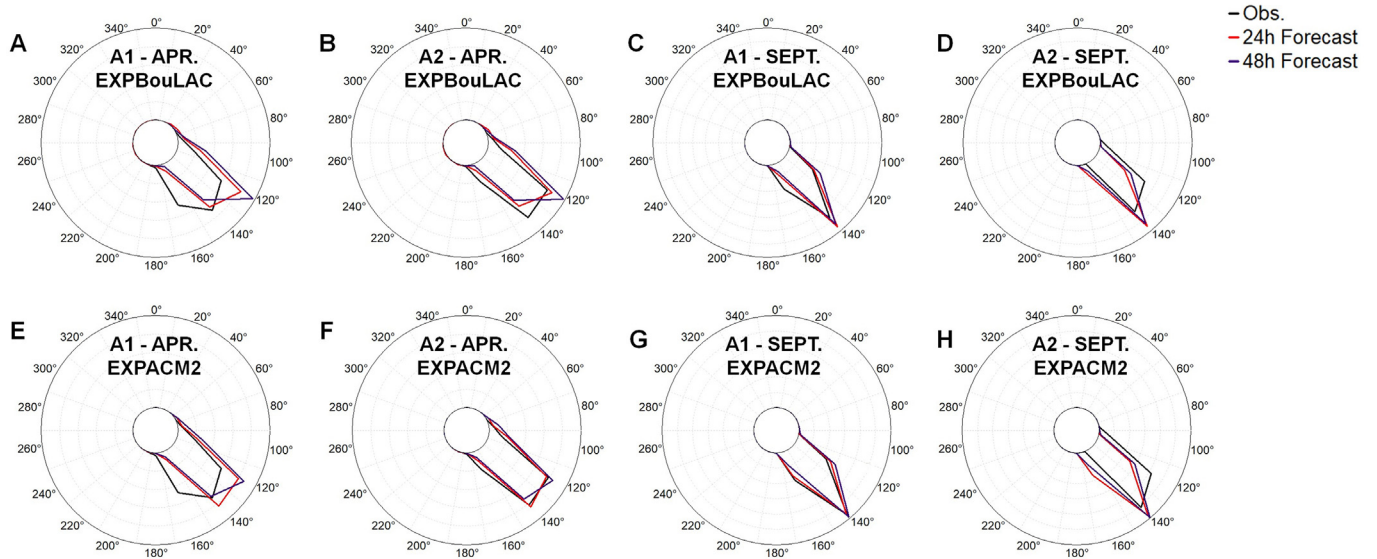


**Fig. 8.** Wind roses of observation data (black solid line), 24 h forecast lead time (red solid line) and 48 h forecast lead time (blue solid line) for the A1 and A2 experiment areas. (For interpretation of the references to colour in this figure legend, the reader is referred to the Web version of this article.)

**Table 2**  
Model skill scores for direction prediction.

<b>EXPBouLAC</b>								
	<u>BIAS<sub>24h</sub></u> (°)	<u>BIAS<sub>48h</sub></u> (°)	<u>MAE<sub>24h</sub></u> (°)	<u>MAE<sub>48h</sub></u> (°)	<u>RMSE<sub>24h</sub></u> (°)	<u>RMSE<sub>48h</sub></u> (°)	<u>MAPE<sub>24h</sub></u> (%)	<u>MAPE<sub>48h</sub></u> (%)
A1-APR.	-9	-14.4	18.6	17.7	29	22.1	21.5	16.4
A2-APR.	-3.9	-9.4	15.8	13.6	28	18.4	21.5	14.2
A1-SEPT.	-2.6	-4.2	5.9	6.8	7.5	9	5.39	6.4
A2-SEPT.	8.6	7	9.5	8.9	11.2	10.9	8.6	8.5
<b>EXPACM2</b>								
	<u>BIAS<sub>24h</sub></u> (°)	<u>BIAS<sub>48h</sub></u> (°)	<u>MAE<sub>24h</sub></u> (°)	<u>MAE<sub>48h</sub></u> (°)	<u>RMSE<sub>24h</sub></u> (°)	<u>RMSE<sub>48h</sub></u> (°)	<u>MAPE<sub>24h</sub></u> (%)	<u>MAPE<sub>48h</sub></u> (%)
A1-APR.	-8.4	-12	14.8	15.9	19.5	20.6	14.5	15.2
A2-APR.	-3.2	-6.8	11.9	12.6	16.8	17.3	13	13.3
A1-SEPT.	-1.4	-3.3	5.3	6.5	6.8	8.7	4.9	6.2
A2-SEPT.	9.8	7.8	10.3	9.3	11.8	11.2	9.2	8.7

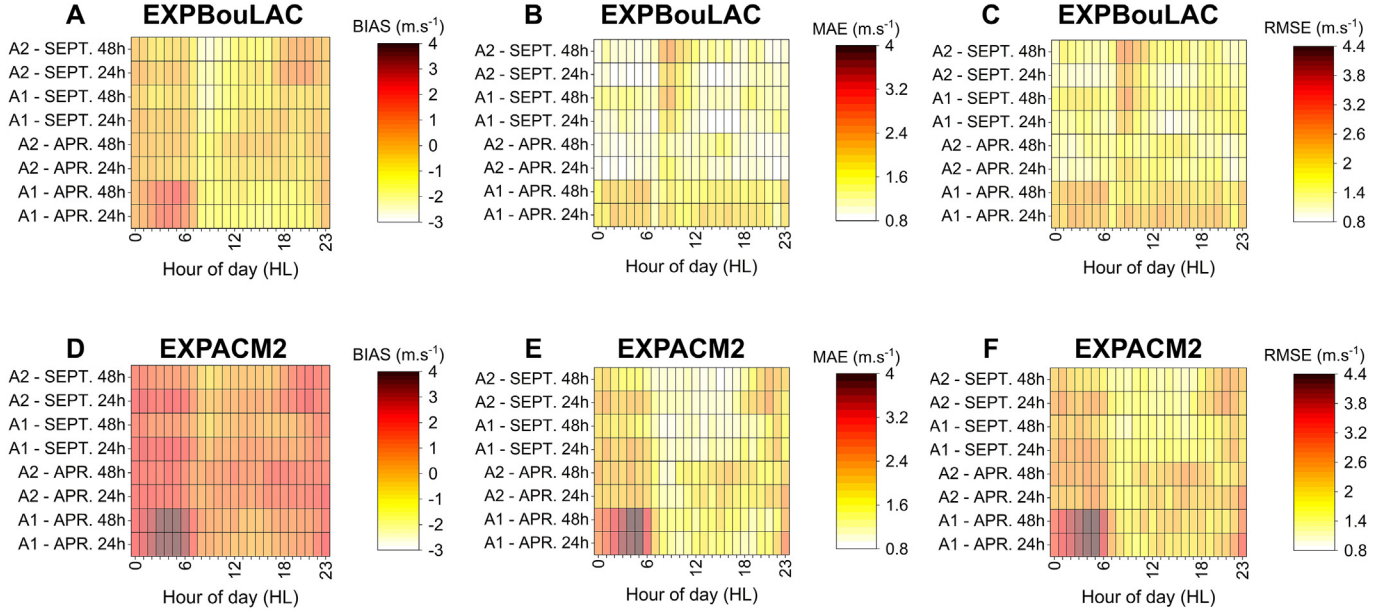
#### 4.4. Diurnal cycle of the wind speed forecasts

Fig. 9 shows skill scores for the diurnal cycle of wind speed at A1 and A2 wind farms for both April and September months. The forecasts of wind speed in EXPBouLAC exhibited a negative BIAS during most part of the day, with the largest errors ( $>2 \text{ m s}^{-1}$ ) occurring between 8:00 to 11:00 HL (11:00 to 14:00 UTC), which are most evident in the mornings of spring (September) (Fig. 9A). On the contrary, wind speeds in EXPACM2 are overestimated most part of the day, especially at nights of autumn when the largest errors ( $>3 \text{ m s}^{-1}$ ) occur between 21:00 to 6:00 HL (00:00 to 9:00 UTC) (Fig. 9D). During the night at both sites the winds are relatively calm because the thermal turbulence ceases after sunset, however, the forecast wind speeds in EXPACM2 are much higher than the observations, indicating the model has not captured the decoupling between the surface and higher-level air after sunset (Fig. 9D, F). In general, PBL schemes that do not have a prognostic equation for TKE such as EXPACM2 tend to produce higher wind speeds, especially in the nighttime period during very stable conditions [33]. The daily–night wind speed cycle is well reproduced by both experiments with the best results in dry (rainy) season for the 24 h lead time (48 h) runs. This suggests that the model needs

more spin up time to adjust to the wind patterns of rainy season (April). For the EXPBouLAC, nighttime wind speeds correspond to relatively smaller errors (MAE and RMSE) while relatively larger errors (RMSE) on the order of  $3 \text{ m s}^{-1}$  are found in EXPACM2. On the other hand, for the daytime period, EXPACM2 performs slightly better the wind maxima in the morning hours (9:00 to 10:00 HL), with RMSE on the order of  $1.2 \text{ m s}^{-1}$  ( $1.6 \text{ m s}^{-1}$ ) in the dry (rainy) season in comparison to the RMSE on the order of  $2.2 \text{ m s}^{-1}$  ( $1.6 \text{ m s}^{-1}$ ) with EXPBouLAC (Fig. 9C, F). In general, both experiments are able to capture the main features of the diurnal cycle of wind speed, however it still has some deficiencies in representing the maximum and minimum peak values observed.

#### 4.5. Evaluating forecast accuracy for different atmospheric stability conditions

To check if WRF wind speed forecast errors are dependent on atmospheric stability, verification of both experiments during different static stability conditions was done (Fig. 10). Static stability in the PBL was assessed by evaluating the vertical gradient of the potential temperature ( $\theta$ ) between 30 and 100 m AGL, as it was done in Ref. [35]. Therefore, PBL was categorized as unstable if



**Fig. 9.** Panels of BIAS, MAE, and RMSE calculated for the mean diurnal cycle of wind speed at 95 m AGL for the A1 and A2 experiment areas and for the both forecast lead times (24 and 48 h).

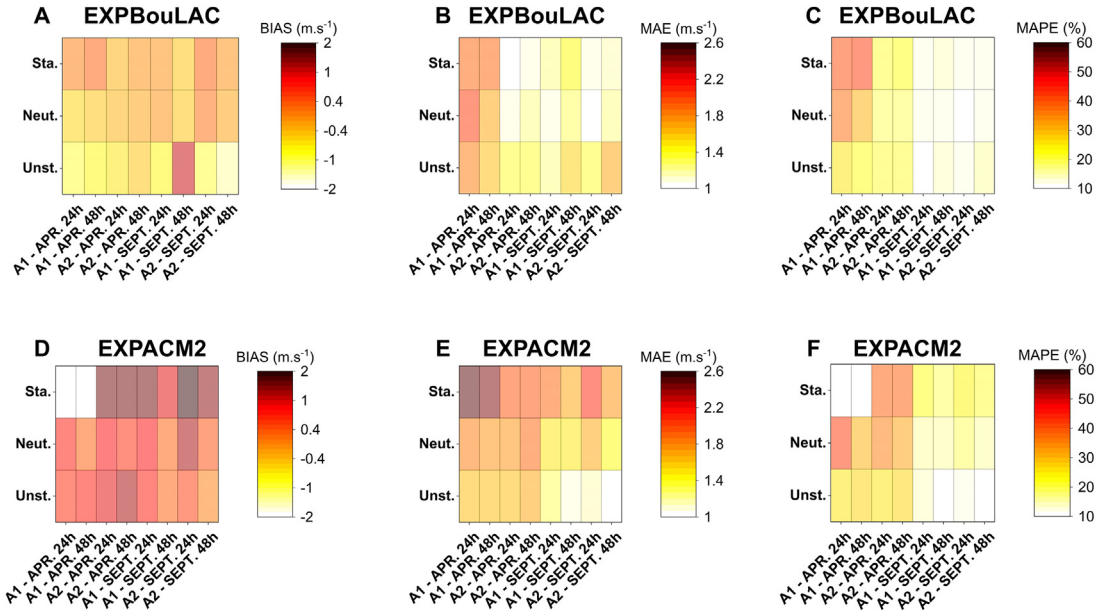


**Fig. 10.** Panels of BIAS, MAE, and RMSE for different atmospheric stability classes at different forecast lead times (24 and 48 h).

$\frac{d\theta}{dz} < 0$ , neutral if  $\frac{d\theta}{dz} = 0$  and stable if  $\frac{d\theta}{dz} > 0$ . Wind speeds are overestimated by both experiments during stable conditions, with higher absolute values ( $\text{BIAS} > 2 \text{ m s}^{-1}$ ) in the EXPACM2 (Fig. 10A, D). This result is in agreement with what is found in Ref. [36], which has shown that non-local schemes (ACM2) tend to produce higher wind speeds than local schemes (BouLAC), especially in the nighttime period. The EXPBouLAC perform best under neutral and stable conditions, with mean (across both seasons and lead times) MAE values of  $1.3 \text{ m s}^{-1}$  and  $1.4 \text{ m s}^{-1}$ , respectively. In addition, MAPE results show remarkable improvement in the EXPBouLAC for all stability classes in comparison to EXPACM2, especially under stable conditions (nearly 14% improvement in forecast skill). However, MAPE results for both the experiments and lead time's locations showed

that model accuracy slightly increases during unstable and neutral conditions when compared to the stable conditions. Our results suggested some limitations of the model performance in stable conditions, which are related to the intermittent turbulence that is a characteristic feature of stable atmospheric conditions at night and still represents a great challenge for numerical models [37].

#### 4.6. Evaluating wind speed dependence

Fig. 11 shows the behavior of both WRF experiments depending on wind speed. The entire study period of both months was divided into hours with the observed wind speed stronger and weaker than  $6 \text{ m s}^{-1}$  (April) and  $9 \text{ m s}^{-1}$  (September). This threshold was chosen

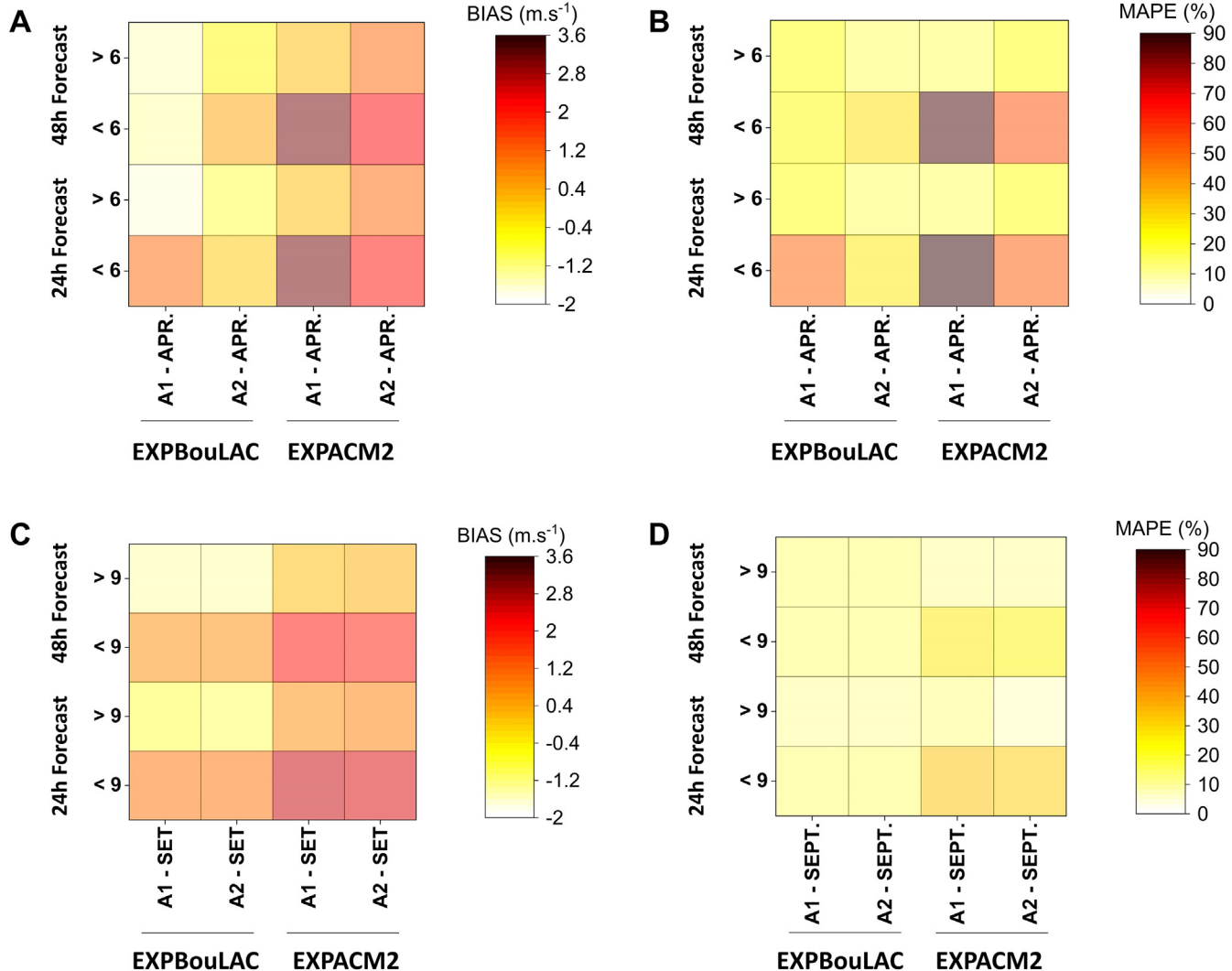


**Fig. 11.** Panels of BIAS, MAE, and RMSE for wind speed higher and lower than  $6 m \cdot s^{-1}$  (april month) and  $9 m \cdot s^{-1}$  (september month) at different forecast lead times (24 and 48 h).

because  $6 m \cdot s^{-1}$  ( $9 m \cdot s^{-1}$ ) was the approximate average wind speed in both wind farms over the study period of April (September) month. We note that MAPE values for April (Fig. 11B) are much better during strong wind episodes (15%–23%) than for wind speed  $< 6 m \cdot s^{-1}$  (24.9%–88.7%). Furthermore, when considering only wind speeds lower than  $6 m \cdot s^{-1}$ , EXPBouLAC improves forecast accuracy by around 30% as compared to EXPACM2. Nevertheless, there is a systematic overestimation/underestimation of wind speed in both EXPACM2 (BIAS  $> 3 m \cdot s^{-1}$ ) and EXPBouLAC ( $-1.5$  up to  $1.2 m \cdot s^{-1}$ ) for speeds  $< 6 m \cdot s^{-1}$  at the wind farms. Analysis suggests that, for the dry period (September), both experiments produced a similar performance for wind speeds greater than  $9 m \cdot s^{-1}$  (MAPE varying between 11 and 14.5%); the worst model performance with highest MAPE values in this season were observed in EXPACM2 (MAPE  $> 30\%$ ; BIAS  $> 2.5 m \cdot s^{-1}$ ) during low wind speed ( $< 9 m \cdot s^{-1}$ ) episodes (Fig. 11D). In general, the mean BIAS of EXPBouLAC tend to overestimate/underestimate magnitudes smaller than the EXPACM2, with values of, respectively,  $1 m \cdot s^{-1}$  (24 h forecast lead) and  $0.8 m \cdot s^{-1}$  (48 h forecast lead) for wind speeds  $< 9 m \cdot s^{-1}$  up to values of  $-0.9 m \cdot s^{-1}$  (24 h forecast lead) and  $-1.4 m \cdot s^{-1}$  (48 h forecast lead) for wind speeds  $> 9 m \cdot s^{-1}$ . Let us mention that, according to the results exposed in Ref. [36], it is possible that this systematic overestimation (underestimation) of

wind speed could be related to the underestimation (overestimation) of friction losses at low boundary layer levels, causing overestimation (underestimation) of wind speed at 95 m AGL. Another plausible reason could be related to the lack of representation of the unresolved topography, which may lead to a general overestimation of wind speed in the model. However, other sources of the uncertainty (model deficiencies) could be the inaccuracy of available GFS data, poor model physics and the inherent limitations of mesoscale model predictability for wind speed at the lower boundary layer. Although it would be interesting to explore the effect of all these sources of errors, such investigations are out of the scope of this study.

#### 4.7. Wind power forecast

Figs. 12 and 13 shows hourly wind power production (kWh) at both wind farms (for a single wind turbine Vestas V100 [26]) and lead times for April and September 2017, respectively. Fig. 12 shows that EXPACM2 tends to overestimate wind power production, whereas EXPBouLAC slightly underestimates it. We also see in Fig. 12 that the monthly average NMAE is approximately 7% larger in the EXPACM2 (NMAE ~ 29%) compared to EXPBouLAC (21.8%) at the A1 site, while for A2 site it substantially decreases from 27.1%

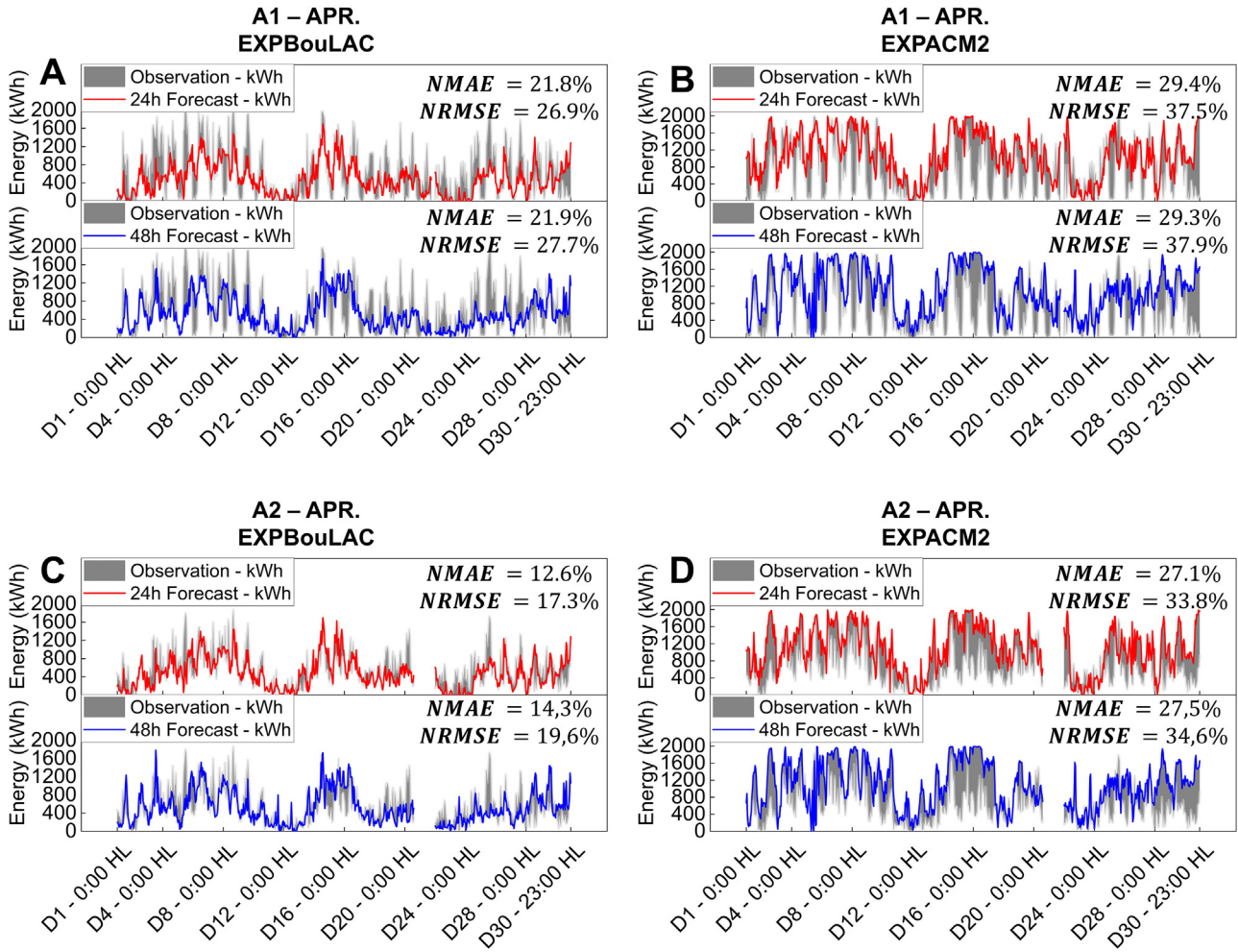


**Fig. 12.** Hourly power in kWh generated by Vestas V100 - 2 MW wind turbine, with observed wind speed data (black line), 24 h forecast lead time (red line) and 48 h forecast lead time (blue line). (For interpretation of the references to colour in this figure legend, the reader is referred to the Web version of this article.)

(EXPACM2) to 12.6% (EXPBouLAC). For both lead times, the NRMSE of EXPBouLAC (Fig. 12) was lower than that of EXPACM2 (nearly 10–15% lower). The best result was for the lead time of 24 h for EXPBouLAC in the A2 site, with a NMAE of 12.6% and NRMSE of 17.3% (Fig. 12C), the largest NMAE and NRMSE was, respectively, 29.3% and 37.9% for the lead time of 48 h with the EXPACM2 in the A1 site (Fig. 12B). Similarly, by comparing both experiments in Fig. 13, we see how the errors (NMAE and NRMSE) decreases as a function of changing season (from rainy-April to dry-September), indicating a better performance of short-term wind power forecasting in September than in April 2017. For example, in the EXPBouLAC forecasting system, the NMAE (NRMSE) in September ranges from about 13.3% to 17.9% (17.7%–23.3%) (Fig. 13A, C), depending on the forecast lead time and wind farm site, being the errors in the later one clearly bigger. In addition, similar to EXPBouLAC, in the EXPACM2 forecasting system the NMAE (NRMSE) ranges from 13.8% to 15.2% (21.2%–23.1%) (Fig. 13B, D). In general, changing from EXPBouLAC to EXPACM2 as the forecasting model generally increased NMAE and NRMSE for 24 h forecast lead time, regardless of the season. Overall, EXPBouLAC-based forecasting has smaller NRMSE due to decreased NMAE as compared to EXPACM2-based forecasting. Lastly, a simplified power production calculation showed that especially in the 24 h forecast lead, power estimated based on the EXPBouLAC are in better agreement with the operational data from the turbine than estimates based on

EXPACM2.

## 5. Conclusions

A pioneering study evaluating the feasibility of using WRF model as a wind energy forecast tool for two real wind farms in the Northeast Brazil was presented. A total of thirty-two sensitivity experiments were conducted by varying different PBL, radiation, convection, and microphysics schemes, and land-surface models during two contrasting seasonal wind regimes (autumn with light winds vs spring with high winds) aiming to find the optimal setup of the model over the region under study. In addition, short-term day ahead forecasting (24–48 h) encompassing two months (April and September 2017), with two configurations based on the best scores obtained in the sensitivity analyses at different lead times, have been performed and validated with real data.

The analyses developed show that, despite the inherent limitations of all parameterizations, the Thompson (microphysics), New Goddard (radiation), Betts-Miller (convection) schemes and Pleim-Xiu (land-surface model) provided the best scores among the schemes investigated. However, the PBL schemes are the most sensitive to wind speed forecasting, producing differences higher than  $2 \text{ m s}^{-1}$  between each other. Comparison of the PBL results revealed that the TKE BouLac scheme followed by nonlocal ACM2 scheme exhibited the best scores overall.

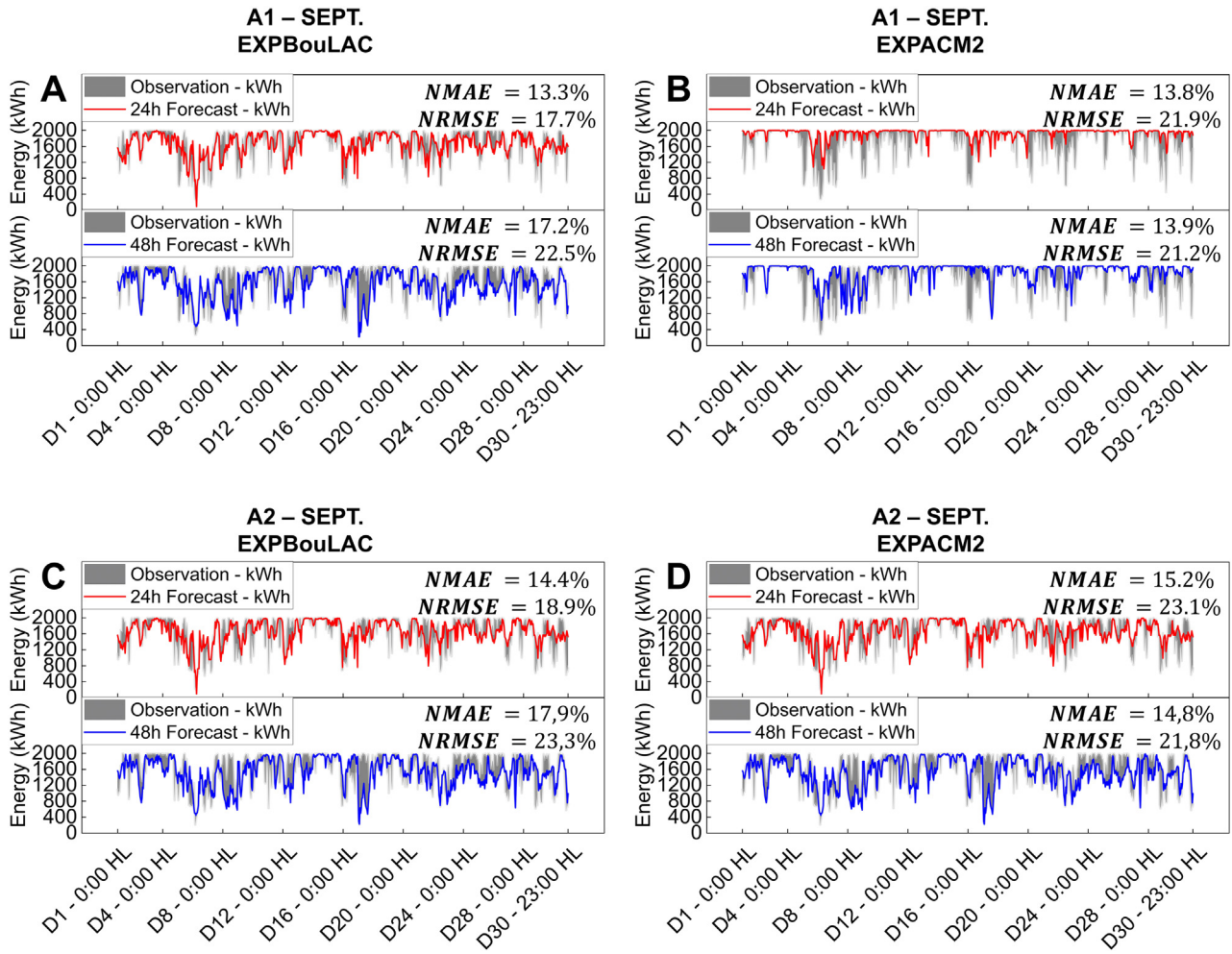


**Fig. 13.** Hourly power in kWh generated by Vestas V100 - 2 MW wind turbine, with observed wind speed data (black line), 24 h forecast lead time (red line) and 48 h forecast lead time (blue line). (For interpretation of the references to colour in this figure legend, the reader is referred to the Web version of this article.)

In general, it has been found that for wind speed forecasting, TKE scheme in EXPBouLAC were in better agreement with observations, both qualitatively and quantitatively ( $MAE < 1.9 \text{ m s}^{-1}$ ). The results furthermore show a seasonal dependence and increases with the lead time, with monthly mean maximum MAE values of  $1.9 \text{ m s}^{-1}$  (EXPBouLAC) and  $2.1 \text{ m s}^{-1}$  (EXPACM2), in the autumn season (i.e., April 2017). Overall, MAPE values presented a better (worst) performance for September (April), and this can be explained by the fact that, in rainy seasons, the large-scale processes (such as ITCZ) have a larger influence compared to spring because wind speed variability increases. The wind speed errors also exhibit strong diurnal patterns in each cycle with a growing trend during the day-time (night-time) hours on the EXPBouLAC (EXPACM2), peaking in spring (autumn) with MAE values of  $2.5 \text{ m s}^{-1}$  ( $4 \text{ m s}^{-1}$ ) at 9:00 HL (5:00 HL). Possible causes of the observed trends in the maximum and minimum wind speeds errors include the poor quality of initialization conditions and/or inaccurate representation of induced turbulence intensity as well as surface roughness in the surface layer.

Another important finding is that the verification depends markedly on wind speed. In fact, MAPE was much lower during strong wind episodes. The error metrics based on BIAS and MAPE demonstrates that EXPBouLAC produced smaller errors during high and low wind regimes compared to EXPACM2 in both sites and

months. We also note that model performance is strongly dependent on atmospheric stability changes. The poorest results were under stable conditions. Model skill is better under neutral and stable conditions in EXPBouLAC than in EXPACM2, while under unstable conditions the results are comparable for both experiments. With regard the errors for power output, the best NRMSE has a month average value of 12.6%, which is an acceptable error margin for allowing the use of the forecasted values in electric market operations. It was also concluded that both experiments generally produces large (lower) errors in power generation when turbulence intensity tends to increase (decrease) during rainy (dry) season of the region under study. Nevertheless, the effect of turbulence in power generation is not completely understood and needs to be investigated further. Compared to the findings of the other physical options used in literatures, the EXPBouLAC forecasting system shows slightly better forecast verification statistics for both wind speed and power forecasts in the region under study. Lastly, this study supports the potential benefits of using WRF model as part of wind speed and energy forecast tool for wind-farm operational planning, turbine maintenance operations and grid scheduling, aiming to minimize technical and financial risks for the end-user.

## Credit author statement

**William Duarte Jacondino:** Conceptualization, Methodology, Validation of WRF outputs for wind speed: Data curation, Writing – original draft. **Ana Lucia da Silva Nascimento:** Visualization, Investigation, Writing- Reviewing and Editing. **Leonardo Calvetti** and **Gilberto Fisch:** Supervision. **Cesar Augustus Assis Beneti** and **Sheila Radman da Paz:** anemometric data provider.

## Declaration of competing interest

The authors declare that they have no known competing financial interests or personal relationships that could have appeared to influence the work reported in this paper.

## Acknowledgments

The authors would like to acknowledge the National Centre for Environmental Prediction (NCEP) for the 3.9.1.1 version of WRF model and the GFS (ds084.1) dataset that was employed for wind speed forecasting. This article was supported by the Federal University of Pelotas, Brazil and by the Conselho Nacional de Desenvolvimento Científico e Tecnológico (CNPq) (131823/2018-3).

## Appendix. List of abbreviations

ACM2	Asymmetric Convective Model version 2
BouLac	Bougeault-Lacarrere
kWh	Kilowatt-hour
MRF	Medium-Range Forecast Model
MYJ	Mellor-Yamada-Janjic
MYNN 2.5	Mellor-Yamada Nakanishi Niino Level 2.5
MYNN 3rd	Mellor-Yamada Nakanishi Niino Level 3
QNSE	Quasi-normal Scale Elimination
RRTM	Rapid Radiative Transfer Method
RRTMG	Rapid Radiative Transfer Method McIAC
WDM6	WRF Double Moment 6 Classe
WSM3	WRF Single Moment 3 Classe
WSM5	WRF Single Moment 5 Classe
WSM6	WRF Single Moment 6 Classe
YSU	Yonsei University

## References

- [1] Käberger T. Progress of renewable electricity replacing fossil fuels. *Glob Energy Interconnect* 2018;1:48–52. <https://doi.org/10.14171/j.2096-5117.gei.2018.01.006>.
- [2] Associação brasileira de Energia eólica (ABEEólica). Infovento 19 - versão inglês. 2021 [Online]. Retrieved: [http://abeeolica.org.br/wp-content/uploads/2021/02/2021\\_02\\_18\\_InfoVento19.pdf](http://abeeolica.org.br/wp-content/uploads/2021/02/2021_02_18_InfoVento19.pdf).
- [3] Giebel G, Kariniotakis G. Wind power forecasting-a review of the state of the art. *Renew. Energy Forecast. From Model. to Appl.* Elsevier Inc.; 2017. p. 59–109. <https://doi.org/10.1016/B978-0-08-100504-0.00003-2>.
- [4] Foley AM, Leahy PG, Maruglia A, McKeogh EJ. Current methods and advances in forecasting of wind power generation. *Renew Energy* 2012;37:1–8. <https://doi.org/10.1016/J.RENENE.2011.05.033>.
- [5] Storm B, Dudhia J, Basu S, Swift A, Giannanco I. Evaluation of the weather research and forecasting model on forecasting low-level jets: implications for wind energy. *Wind Energy* 2009;12:81–90. <https://doi.org/10.1002/we.288>.
- [6] Shin HH, Hong SY. Intercomparison of planetary boundary-layer parameterizations in the WRF model for a single day from CASES-99. *Boundary-Layer Meteorol* 2011;139:261–81. <https://doi.org/10.1007/s10546-010-9583-z>.
- [7] Deppe AJ, Gallus WA, Takle ES, Deppe AJ, Wag Jr, Takle ES. A WRF ensemble for improved wind speed forecasts at turbine height. *Weather Forecast* 2013;28:212–28. <https://doi.org/10.1175/WAF-D-11-00112.1>.
- [8] Draxl C, Hahmann AN, Peña A, Giebel G. Evaluating winds and vertical wind shear from Weather Research and Forecasting model forecasts using seven planetary boundary layer schemes. *Wind Energy* 2014;17:39–55. <https://doi.org/10.1002/we.1555>.
- [9] Carvalho D, Rocha A, Gómez-Gesteira M, Silva Santos C. Sensitivity of the WRF model wind simulation and wind energy production estimates to planetary boundary layer parameterizations for onshore and offshore areas in the Iberian Peninsula. *Appl Energy* 2014;135:234–46. <https://doi.org/10.1016/J.APENERGY.2014.08.082>.
- [10] Ramos DN da S, Lyra RF da F, Silva Júnior RS da. Previsão do vento utilizando o modelo atmosférico WRF para o estado de Alagoas. *Rev Bras Meteorol* 2013;28:163–72. <https://doi.org/10.1590/S0102-77862013000200005>.
- [11] Pinto LIC, Martins FR, Pereira EB, Fisch GF, Lyra RF da F. Confiabilidade nas estimativas do regime de vento fornecidas pelo brams no estado de Alagoas: influência do aninhamento e da resolução horizontal de grades. *Rev Bras Meteorol* 2014;29:242–58. <https://doi.org/10.1590/S0102-77862014000200008>.
- [12] Tuchtenhagen P, Basso J, Yamasaki Y. Avaliação do potencial eólico no Brasil em 2011 Wind power assessment over Brazil in 2011. 2014. p. 390–401. <https://doi.org/10.5902/2179460X13148>.
- [13] Draxl C, Hodge B-M, Clifton A, McCaa J. Overview and meteorological validation of the wind integration national dataset toolkit. 2015 [Online]. Retrieved, <https://www.nrel.gov/docs/fy15osti/61740.pdf>.
- [14] Hahmann AN, Vincent CL, Peña A, Lange J, Hasager CB. Wind climate estimation using WRF model output: Method and model sensitivities over the sea. *Int J Climatol* 2015;35:3422–39. <https://doi.org/10.1002/joc.4217>.
- [15] Giannaros TM, Melas D, Ziomas I. Performance evaluation of the Weather Research and Forecasting (WRF) model for assessing wind resource in Greece. *Renew Energy* 2017;102:190–8. <https://doi.org/10.1016/j.renene.2016.10.033>.
- [16] Prósper MA, Otero-Casal C, Fernández FC, Miguez-Macho G. Wind power forecasting for a real onshore wind farm on complex terrain using WRF high resolution simulations. *Renew Energy* 2019;135:674–86. <https://doi.org/10.1016/J.RENENE.2018.12.047>.
- [17] Jacondino WD, Calvetti L, Nascimento ALDS, Beneti CAA, da Paz SR, Jadalla OM. Statistical analysis of wind in two wind farms in Rio Grande do Norte. *Anu do Inst Geociencias* 2019;42. [https://doi.org/10.11137/2019\\_2\\_230\\_244](https://doi.org/10.11137/2019_2_230_244).
- [18] Alvares CA, Stape JL, Sentelhas PC, De Moraes Gonçalves JL, Sparovek G. Köppen's climate classification map for Brazil. *Meteorol Z* 2013;22:711–28. <https://doi.org/10.1127/0941-2948/2013/0507>.
- [19] Lucena RL, Cabral Júnior JB, Steinke ET. The hydroclimatological behavior of the Brazilian state of Rio Grande do Norte and the municipality of Caicó. *Rev Bras Meteorol* 2018;33:485–96. <https://doi.org/10.1590/0102-7786333008>.
- [20] Rao VB, De Lima MC, Franchito SH. Seasonal and interannual variations of rainfall over eastern northeast Brazil. *J Clim* 1993;6:1754–63. [https://doi.org/10.1175/1520-0442\(1993\)006<1754:saior>2.0.co;2](https://doi.org/10.1175/1520-0442(1993)006<1754:saior>2.0.co;2).
- [21] thiesclima.com - products n.d. <https://www.thiesclima.com/en/Products/Wind/>. [Accessed 12 October 2020].
- [22] Skamarock W, Klemp J, Dudhia J, Gill D, Barker D, Duda M, Huang X, Wan W, Powers y J. A description of the advanced research WRF version 3. 2008 [Online]. Retrieved: [http://www2.mmm.ucar.edu/wrf/users/docs/arw\\_v3.pdf](http://www2.mmm.ucar.edu/wrf/users/docs/arw_v3.pdf).
- [23] Pennelly C, Reuter G, Flesch T. Verification of the WRF model for simulating heavy precipitation in Alberta. *Atmos Res* 2014;135–136:172–92. <https://doi.org/10.1016/j.atmosres.2013.09.004>.
- [24] Sikder S, Hossain F. Assessment of the weather research and forecasting model generalized parameterization schemes for advancement of precipitation forecasting in monsoon-driven river basins. *J Adv Model Earth Syst* 2016;8:1210–28. <https://doi.org/10.1002/2016MS000678>.
- [25] Jee J-B, Kim S. Sensitivity study on high-resolution WRF precipitation forecast for a heavy rainfall event. *Atmosphere* 2017;8:96. <https://doi.org/10.3390/atmos8060096>.
- [26] Dzebre DEK, Adaramola MS. A preliminary sensitivity study of Planetary Boundary Layer parameterisation schemes in the weather research and forecasting model to surface winds in coastal Ghana. *Renew Energy* 2020;146:66–86. <https://doi.org/10.1016/j.renene.2019.06.133>.
- [27] Wei Wang CB, Duda Michael, Dudhia Jimy, Gill Dave, Kavulich Michael, Kelly Keene, Chen Ming, Lin Hui-Chuan, Michalakes John, Rizvi Syed, Zhang Xin, Berner Judith, Soyoung Ha and kate fossell, ARW version 3 modeling system user's guide. 2016.
- [28] Datasheet Vistas V100-2.0. 2020 [Online]. Retrieved: <http://abeeolica.org.br/wp-content/uploads/2020/09/Infowind17.pdf>.
- [29] Hanna SR, Yang R. Evaluations of mesoscale models' simulations of near-surface winds, temperature gradients, and mixing depths. *J Appl Meteorol* 2001;40:1095–104. [https://doi.org/10.1175/1520-0450\(2001\)040<1095:EOMMSO>2.0.CO;2](https://doi.org/10.1175/1520-0450(2001)040<1095:EOMMSO>2.0.CO;2).
- [30] Staid A, Pinson P, Guikema SD. Probabilistic maximum-value wind prediction for offshore environments. *Wind Energy* 2015;18:1725–38. <https://doi.org/10.1002/we.1910>.

10.1002/we.1787.

- [31] Thompson G, Field PR, Rasmussen RM, Hall WD. Explicit forecasts of winter precipitation using an improved bulk microphysics scheme. Part II: implementation of a new snow parameterization. *Mon Weather Rev* 2008;136: 5095–115. <https://doi.org/10.1175/2008MWR2387.1>.
- [32] Bhattacharya A, Mandal M. Evaluation of Noah land-surface models in predicting soil temperature and moisture at two tropical sites in India. *Meteorol Appl* 2015;22:505–12. <https://doi.org/10.1002/met.1481>.
- [33] Stergiou I, Tagaris E, Sotiropoulou R-EP. Sensitivity assessment of WRF parameterizations over europe. *Proceedings* 2017;1:119. <https://doi.org/10.3390/ecas2017-04138>.
- [34] Jiménez PA, Dudhia J. On the ability of the WRF model to reproduce the surface wind direction over complex terrain. *J Appl Meteorol Climatol* 2013;52:1610–7. <https://doi.org/10.1175/JAMC-D-12-0266.1>.
- [35] Fernández-González S, Martín ML, García-Ortega E, Merino A, Lorenzana J, Sánchez JL, et al. Sensitivity analysis of the WRF model: wind-resource assessment for complex terrain. *J Appl Meteorol Climatol* 2018;57:733–53. <https://doi.org/10.1175/JAMC-D-17-0121.1>.
- [36] Kleczek MA, Steeneveld GJ, Holtslag AAM. Evaluation of the weather research and forecasting mesoscale model for GABLS3: impact of boundary-layer schemes, boundary conditions and spin-up. *Boundary-Layer Meteorol* 2014;152:213–43. <https://doi.org/10.1007/s10546-014-9925-3>.
- [37] Olsen BT, Hahmann AN, Sempreviva AM, Badger J, Jørgensen HE. An inter-comparison of mesoscale models at simple sites for wind energy applications. *Wind Energy Sci Discuss* 2016;1–32. <https://doi.org/10.5194/wes-2016>.